

RSC Advances



This is an *Accepted Manuscript*, which has been through the Royal Society of Chemistry peer review process and has been accepted for publication.

Accepted Manuscripts are published online shortly after acceptance, before technical editing, formatting and proof reading. Using this free service, authors can make their results available to the community, in citable form, before we publish the edited article. This *Accepted Manuscript* will be replaced by the edited, formatted and paginated article as soon as this is available.

You can find more information about *Accepted Manuscripts* in the [Information for Authors](#).

Please note that technical editing may introduce minor changes to the text and/or graphics, which may alter content. The journal's standard [Terms & Conditions](#) and the [Ethical guidelines](#) still apply. In no event shall the Royal Society of Chemistry be held responsible for any errors or omissions in this *Accepted Manuscript* or any consequences arising from the use of any information it contains.

ARTICLE

xylene gas sensor based on α -MoO₃/ α -Fe₂O₃ heterostructure with high response and low operating temperature

Cite this: DOI: 10.1039/x0xx00000x

Received 00th January 2012,
Accepted 00th January 2012

DOI: 10.1039/x0xx00000x

www.rsc.org/

Dingsheng Jiang^a, Wei Wei^b, Feng Li^b, Yujia Li^a, Caixia Liu^{b,*}, Dongming Sun^a,
Caihui Feng^{c,*}, Shengping Ruan^{a,*}

α -MoO₃/ α -Fe₂O₃ nanostructure composites were fabricated via a facile and low-cost hydrothermal strategy. X-ray diffraction (XRD), scanning electron microscopy (SEM), Transmission electron microscope (TEM) and Energy Dispersive X-Ray Spectroscopy (EDX) were used to characterize the samples. The results revealed that the α -Fe₂O₃ nanorod grew on the surface of α -MoO₃ nanobelts. The result shows the length and the width of α -MoO₃ nanobelts is about 6 μ m and 200 nm. The average length of α -Fe₂O₃ nanorod was 10 nm. The sensing properties towards various kinds of gases were tested and the heater-type gas sensors based on α -MoO₃ nanobelts and α -MoO₃/ α -Fe₂O₃ nanostructure composites showed excellent performance towards xylene. It was found that such heterostructure composites exhibited an enhanced xylene sensing properties compared with α -MoO₃ nanobelts. For example, at a xylene concentration of 5 ppm, the response of the α -MoO₃/ α -Fe₂O₃ composites was 4.79, which was about 3 times higher than that of α -MoO₃ nanostructures at 206°C.

Introduction

In recent years, gas sensors have attracted the attention all over the world due to its function of detecting pollutant and toxic gases. It is well known that the response, selectivity, times of response and recovery are the most important parameters in producing gas sensors. Therefore, it's essential for human to improve these parameters by developing new methods.

Xylene mainly comes from chemical engineering materials such as painting and adhesive in the indoor environment. As one of the most serious pollutants among volatile organic compounds (VOCS), even microscale of xylene has tremendous damage to human being and careless oral of xylene can cause horrible diseases such as acute pneumonia and cancer. Thus, it is significant to detect and measure the existence and the content of xylene. Hitherto, various effective methods such as micro fabricated preconcentrator technology¹, solid-state chemical technology², double-layered metal-oxide thin film technology³ have been used to detect xylene. However, these methods have disadvantages of slow response speed, bulky machine and danger to body, etc^{2, 4, 5}. Metal oxide semiconductor demonstrates the advantages of low cost, facile method, easy fabrication, fast response and recovery time.

One dimensional (1D) nanostructure oxide semiconductors such as nanotubes, nanowires, nanofibers and nanobelts have received much attention. Plenty of methods such as electrospinning, vapor-solid and hydrothermal synthesis were used to prepare 1D nanostructure materials during the past decades. One-dimension nano-products

play an important role in gas sensing owing to the advantages of high surface. High ratio of surface to volume can achieve higher response comparing with that of low ratio.

As important functional materials, α -MoO₃ has been investigated and applied in catalyst⁶⁻⁹, solar cell¹⁰⁻¹², light-emitting diodes^{13, 14}, capacitors¹⁵⁻¹⁷, gas sensors and optical detectors. In recent years, α -MoO₃ has been one of the most newly-developing n-type metal oxide semiconductors which can detect toxic gas. α -MoO₃ is an n-type semiconductor with a wide band gap of 3.2 eV and has been investigated for ethanol¹⁸, NO₂¹⁹, H₂S²⁰, H₂¹², TMA²¹, C₂H₅OH₂₄²² and xylene detection. α -Fe₂O₃ is a p-type semiconductor with a band gap of 2.2 eV. It is found that α -MoO₃/ α -Fe₂O₃ has improved the performances compared with α -MoO₃ nanobelts. Therefore, the preparation of α -MoO₃/ α -Fe₂O₃ composites has great scientific and practical significance.

In this paper, α -MoO₃ nanobelts covered with α -Fe₂O₃ were successfully prepared via two steps hydrothermal reactions. Gas sensors based on α -MoO₃/ α -Fe₂O₃ composites were fabricated to explore the potential applications. The gas sensing properties based on α -MoO₃/ α -Fe₂O₃ composites were investigated for detecting xylene. Heater-type sensors based on α -MoO₃/ α -Fe₂O₃ composites performed a high response to xylene comparing with sensors of α -MoO₃ nanobelts at a low operating temperature of 206 °C which is lower than that of most other sensors^{2, 5, 12, 23}.

Experimental

Synthesis of α -MoO₃ nanobelts

All of the chemical reagents are analytical grade without any further purification. α -MoO₃ nanobelts were synthesized via a facile hydrothermal procedure. Briefly, 0.618g of ammonium heptamolybdate tetrahydrate ((NH₄)₆Mo₇O₂₄·4H₂O) was dissolved into 25 ml of deionized water with vigorous stirring to form aqueous solution (0.02 M). Then 2.5 ml of nitric acid (HNO₃) was slowly dropwise-added into the aqueous solution. The resulting solution was transferred into a Teflon-lined stainless steel autoclave of 50 ml capacity with hydrothermal treatment for 36 h at 180 °C. After the autoclave was cooled down to room temperature naturally, white precipitation was collected by centrifugation for several times before dried at 60 °C for 12 h. Finally the products were then annealed at 300 °C for 2 h at the speed of 1 °C /min to obtain the light yellow α -MoO₃ nanobelts.

Syntheses of α -MoO₃/ α -Fe₂O₃ nanorods

α -Fe₂O₃ nanorods were synthesized by a surfactant-free hydrothermal strategy. In a typical experimental procedure, 0.05 g of the above α -MoO₃ nanobelts were dispersed in 16 ml of deionized water with continuous stirring vigorously to form suspension. Then, 0.054 g of FeCl₃ · 6H₂O and 0.028 g of Na₂SO₄ · 10H₂O were dropwise-added into the suspension, respectively. After stirring, the suspension was transferred into a Teflon-lined stainless steel autoclave of 50 ml capacity with hydrothermal treatment for 10 h at 120 °C. The resulting precipitation was collected by centrifugation with deionized water and ethanol for several times, and dried at 60 °C for 12 h. Finally, red powder was obtained by annealing the above precipitates at a heating rate of 1°C/min to 500 °C for 2 h. The specimen was collected for the further characterization.

Characterization

X-ray diffraction patterns were gained to measure the phase identification and the crystal sizes by XRD analysis (Rigaku TTRIII X-ray diffractometer with Cu K α 1 radiation (λ =1.5406 Å) in the 2 theta range of 20-80°). The morphologies of the samples were achieved by scanning electron microscopy (JEOL JSM-7500F microscope operating at 15 kV). Transmission electron microscopy (TEM) and high-resolution transmission electron microscopy (HRTEM) images were obtained by TEM instrument and the Energy Dispersive X-Ray Spectroscopy (EDX) image was received to measure the composition of the materials.

Fabrication and measurement of gas sensors

Sensor devices were fabricated by the similar method in our previous work^{24, 25}. The composites prepared were mixed with deionized water at a weight ratio of 1:4 and grinded for a while. Then the specimens were coated onto the external of the ceramic tube which was attached with a pair of parallel golden electrodes using a writing brush. The Ni-Cr alloy heating coil was inserted through the ceramic tube and the heating conduction part of the heating coil was completely fixed. The structure of sensors is showed in fig. 1.

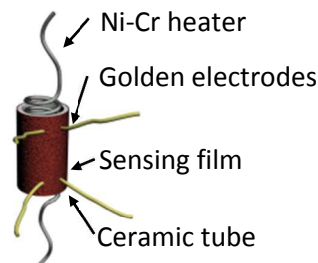


Fig. 1 structure of heater-type gas sensor after coating sensing film

The working temperature was adjusted via electric current which was given by the CGS-8 Intelligent Gas Sensing Analysis System (Beijing Elite Tech Co., Ltd., China). Test gases were injected into the glass containers by micro injections from air bags. The response of the gas sensors was defined and measured as Ra (the resistance of the sensors in the air) /Rg (the resistance of the sensor in the test gas). The response time is defined as the period in which the resistance of sensors reach from 10 % to 90 % of the steady value when exposed to test gases, while the recovery time is defined as the period in which the resistances of sensors reach from 90 % to 10 % of the steady value after exposed to oxygen²⁶.

Result and discussion

Materials characterization

Fig. 2 shows the crystal structure and the phase identification of the prepared materials identified by X-ray diffraction (XRD). All the peaks were matched well with standard XRD patterns in the Fig. 2(a) and the sample was assigned to pure α -MoO₃ (JCPDS 05-0508) which was prepared in our previous work²⁵. For the composites, the crystal phases were mixed by α -MoO₃ and α -Fe₂O₃. The pattern in Fig. 2(b) shows the residual diffraction peaks were consistent with the standard data file of α -Fe₂O₃ (JCDs 33-0664). No other diffraction peaks corresponding to impurities were observed, which indicated that the product had a high purity.

The morphologies of the nanobelts made in our previous work were showed in fig. 3(a)²⁵. A number of uniform and homogeneous nanobelts were clearly observed. It can be testified that the width of the α -MoO₃ nanobelts were about 200 nm, and the length were about 6 μ m. Moreover, the rough surface of the α -MoO₃ nanobelts was exhibited in fig.3 (b)²⁵. After the growth of α -Fe₂O₃ nanorods on α -MoO₃ nanobelts, the structure was showed in fig. 3(c). The average width and the length of the materials were 250 nm and 6 μ m, respectively. The detail of the structure was showed in Fig. 3(d). It can be seen that the average length of α -Fe₂O₃ nanorod was 10 nm. The typical transmission electron microscopy (TEM) images in fig. 3(e) show that α -MoO₃ nanobelts were surrounded by α -Fe₂O₃ nanorods which stretched outside. Fig. 3(f) shows a high-resolution TEM (HRTEM) image of α -MoO₃/ α -Fe₂O₃ nanostructures. The lattice fringe spacing was observed to be 0.220 nm which corresponding to the plane of (1 1 3) of α -Fe₂O₃. EDX (Energy Dispersive X-Ray Spectroscopy) images in Fig. 3(g) shows the elements constitutions of the materials are O, Mo and Fe, the highest peak in the image represents element of Si which is the substrate of the instrument.

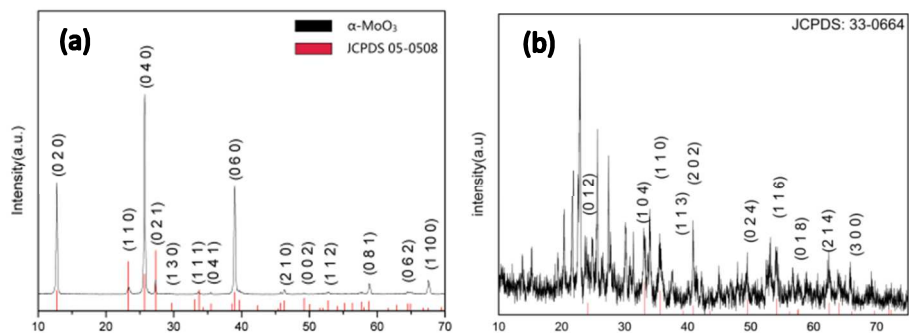


Fig. 2(a) XRD patterns of pure α - MoO_3 nanostructure (b) XRD patterns of α - MoO_3/α - Fe_2O_3 composites

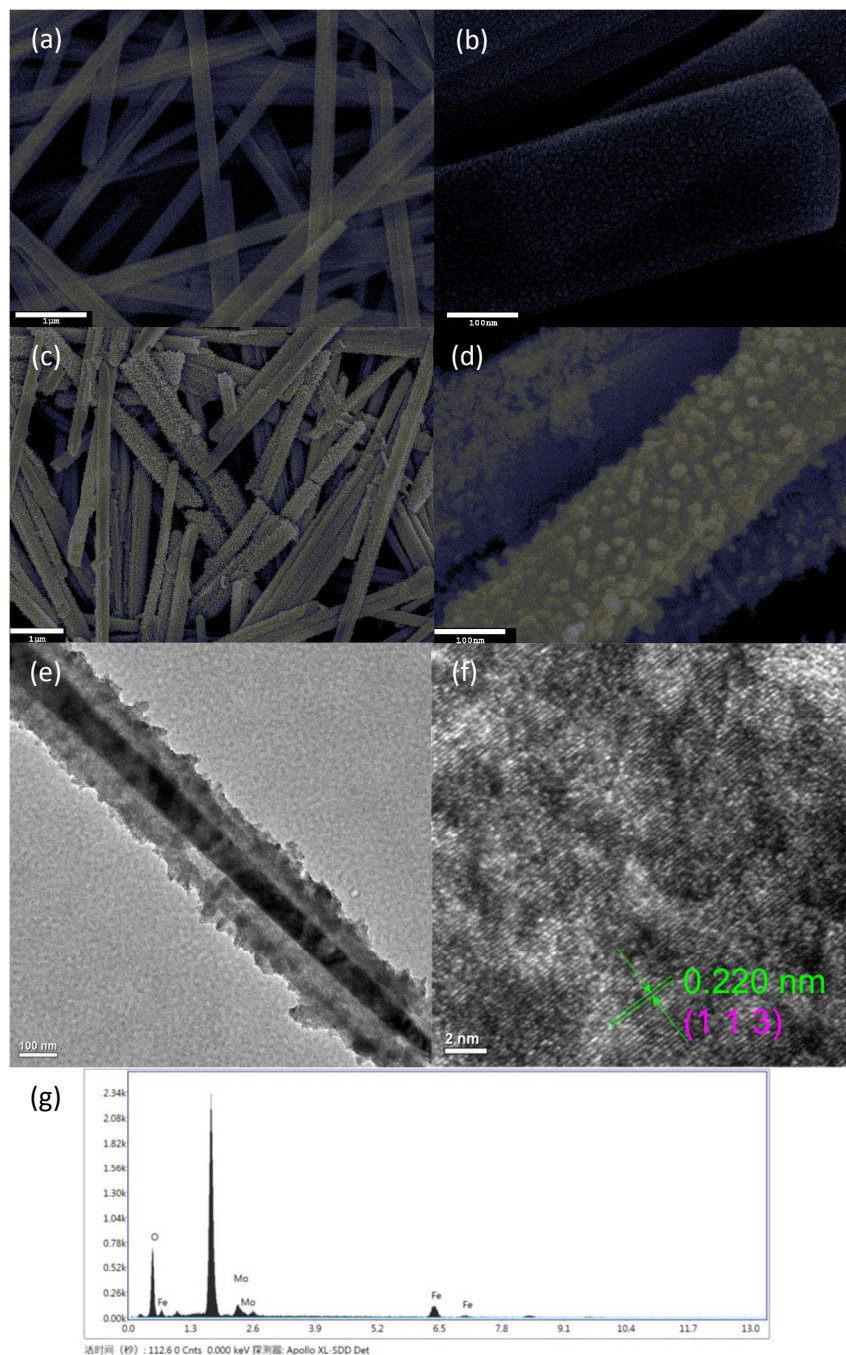


Fig. 3(a-b) Typical SEM images of pure α - MoO_3 nanostructures (c-d) Typical SEM images of pure α - MoO_3/α - Fe_2O_3 composites (e) Typical TEM image of α - MoO_3/α - Fe_2O_3 composites (f) HRTEM image of α - Fe_2O_3 nanorods (g) EDX image of α - MoO_3/α - Fe_2O_3 composites

Sensing properties

The sensors based on α -MoO₃/ α -Fe₂O₃ composites and pure α -MoO₃ nanobelts were fabricated and their sensing properties were investigated. The sensors which were coated with α -MoO₃/ α -Fe₂O₃ composites had a good performance on xylene. Fig. 4 shows the responses of the two kinds of sensors to 100 ppm xylene from 160 °C to 280 °C. It was obvious that the temperature improved the chemical reaction between sensors and test gas because it improves the speed of molecule vibration. However, further increase in temperature resulted in the response of the sensors decreasing from 206 °C to 280 °C. As showed in fig. 5, the reason may be that faster desorption of xylene happened when temperature increasing which caused reduced reaction between xylene and oxygen species on the surface of the materials. Thus, the response of the sensor decreased along with temperature increasing. For the pure α -MoO₃ nanobelts and the α -MoO₃/ α -Fe₂O₃ composites materials, the responses reached maximum value of 3 and 6.8 when temperature was 206 °C, respectively. The optimum working temperature of two sensors were both 206 °C and response of the sensor based on α -MoO₃/ α -Fe₂O₃ core-shell structure was two times higher than that of the sensor based on α -MoO₃ nanobelts at the same optimum temperature. It was obvious that the sensors based on α -MoO₃/ α -Fe₂O₃ composites enhanced the gas sensing.

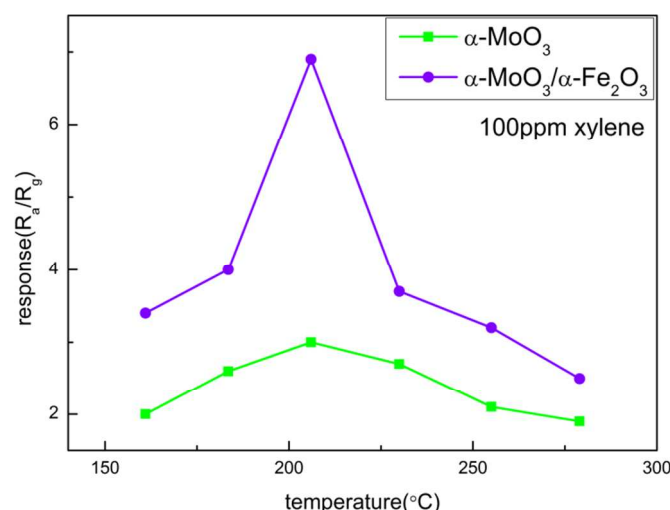


Fig. 4 response of sensors based on α -MoO₃ nanobelts and α -MoO₃/ α -Fe₂O₃ composites to 100 ppm xylene at different temperatures

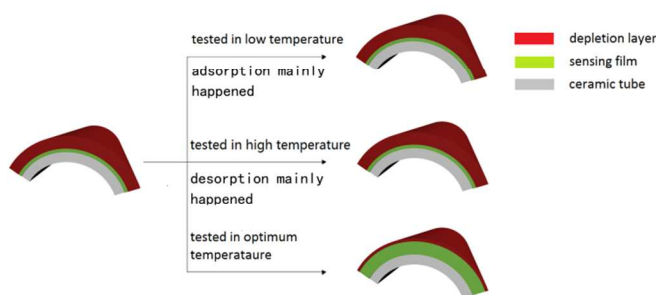


Fig. 5 reaction status of the sensors at different temperatures

Fig. 5 shows the response of the sensors based on α -MoO₃/ α -Fe₂O₃ composites and pure α -MoO₃ nanobelts versus different

concentrations of xylene at 206 °C. For the sensor based on α -MoO₃/ α -Fe₂O₃ composites, the response increased along with the increasing of the concentration of xylene. Furthermore, the response was nearly linearly increasing at the range of 5 to 100 ppm of test gas. The sensors came to saturation when the concentration of xylene gas reached 1000 ppm. Significantly, the response of the sensor is 4.79 towards xylene to the concentration of 5 ppm and it's three times higher than that of pure α -MoO₃ nanobelts. It's obvious that the sensors based on α -MoO₃/ α -Fe₂O₃ composites quite enhanced the response to xylene.

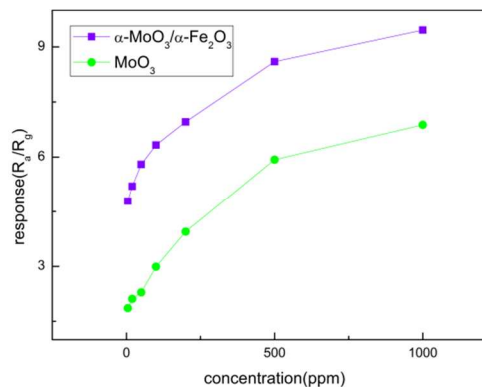


Fig.6 response of sensors based on α -MoO₃ nanobelts and α -MoO₃/ α -Fe₂O₃ composites at 206 °C versus different concentrations of xylene

Selectivity is an important property of gas sensors in the practical application. The responses of the sensors towards different test gases such as methylbenzene, formaldehyde and carbon monoxide were showed in Fig. 7 were tested at 206 °C with a concentration of 100 ppm similarly. The result shows that the response of the sensors based on α -MoO₃ nanobelts towards 100 ppm of xylene could reach 6.8 and less than 1.6 towards other test gases. Therefore, sensors based on α -MoO₃/ α -Fe₂O₃ composites showed better selectivity to xylene contrast with other text gases. However, it is still difficult for us to distinguish the three forms of xylene (o, m, p) at present because of their similar chemical properties.

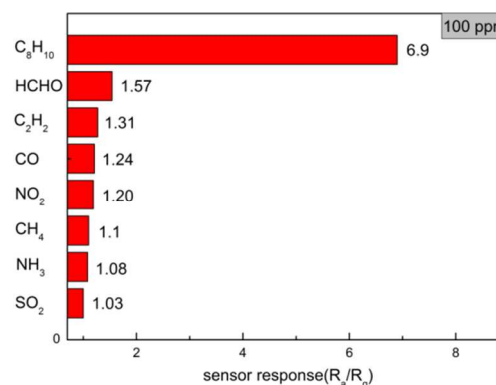


Fig.7 response of sensors based on α -MoO₃/ α -Fe₂O₃ composites at 206 °C towards various test gases

Rapid response and recovery time are significant parameters in designing oxide semiconductor gas sensors. Fig.8 shows the response and recovery time of the sensors towards xylene from 20 ppm to 100 ppm at 206 °C. The figure indicated that the resistance of the sensors decreased rapidly at first and then changed slowly due to the reaction slowed down gradually

when the sensors were transferred from air to xylene. The resistance of the sensors resumed slowly when sensors were exposed to the air. The time of response and recovery were 87 s and 190 s to 100 ppm of xylene, respectively. For pure α - MoO_3 nanobelts, the response and recovery time were 7 s and 87 s, respectively.

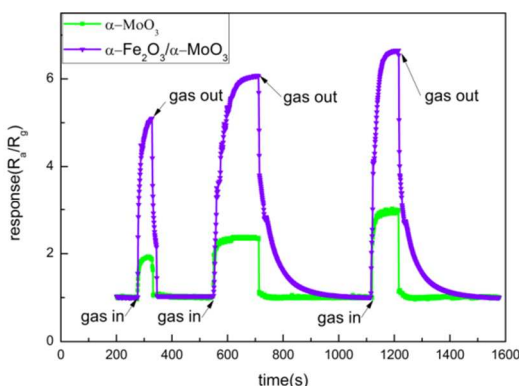
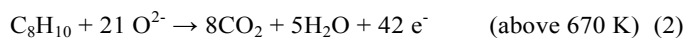
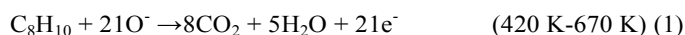


Fig. 8 responses to different concentration of xylene for α - MoO_3 and α - MoO_3/α - Fe_2O_3 composites, respectively

Sensing mechanism of α - MoO_3/α - Fe_2O_3 composites to xylene

As a n-type semiconductor, the sensing performance of α - MoO_3 nanobelts may own to the mechanism of the adsorption and desorption process of gas molecules on the surface of the oxide in the matter of crystal structure²⁷. As is shown in Fig. 9, the formation process of defects in the α - MoO_3 nanobelts is as following: In the step (a), oxygen from the air is attached on the surface of α - MoO_3 nanobelts when α - MoO_3 exposed in the air. Then the oxygen absorb electrons from α - MoO_3 nanobelts and transforms oxygen into O^\cdot (420 K-670 K), O^{2-} (above 670 K), and O_2^\cdot (below 420 K) on the surface of sensing layer which would lead the holes spread all over the surface and cause the resistance increasing. When α - MoO_3 nanobelts are transformed to the test gas (xylene) as showed in step (b) to step (c), the chemical reaction between xylene and the adsorbed oxygen ions can be described as following:



The reaction in the equation (1) above is in ascendancy for the reason of optimum temperature of the sensors. It demonstrates that CO_2 and electrons would be released when the reaction processing. These electrons neutralize the holes in the α - MoO_3 nanobelts in step (4) and cause the decreasing of the resistance of the sensors. The excellent sensing performance makes α - MoO_3/α - Fe_2O_3 a newly potential candidate for the detection of xylene.

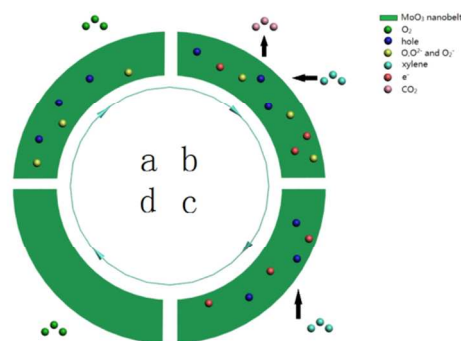


Fig. 9 illustration of sensors based on α - MoO_3 nanobelts sensing performance for xylene

The enhanced performance of sensors based on α - MoO_3/α - Fe_2O_3 core-shell structural composites maybe the result of two factors. First, the fast response of the sensors may attribute to the 1D nanostructure. The ratio of length and width of α - MoO_3 nanobelts could reach as high as 30/1 and the nanobelts were pretty thin, which leads to quick adsorption and desorption of O_2 and xylene consumed at the surface of the sensing layer. Consequently, reaction occurred at sensing surface will be greatly accelerated, which results in faster and higher response of the sensors based on α - MoO_3/α - Fe_2O_3 nanostructural composites. Second, α - MoO_3 and α - Fe_2O_3 are n-type and p-type semiconductors, respectively. The contact of α - MoO_3 and α - Fe_2O_3 will form heterojunction and the energy band structure of heterojunction is depicted in fig. 10. Φ_{eff} represents the effective barrier height. The conductivity (G) of heterojunction can be given in the following at high temperature²⁷

$$G = G_0 \exp(-q \Phi_{\text{eff}} / k_b T) \quad (5)$$

G_0 in the formula is a constant parameter, q is the charge of an electron with the unit of Coulomb (C), k_b is Boltzmann's constant and T represents absolute temperature with the unit of Kelvin (K). So G is decided by the change of Φ_{eff} (eV). The electrons in the conduction bands of the heterojunction are transferred into air so the Φ_{eff} will increase. As shown in fig. 10, the conductivity of the heterojunction is very low because of Φ_{eff} . When the heterojunction is transferred into reducing gases such as ethanol, acetone and xylene, the reaction between heterojunction and gases can release the electron and the electrons were transferred back to the conduction band of the heterojunction as shown in fig. 10, which will lower the height of the barrier potential. Consequently, the conductivity of heterojunction will increase greatly and leads to a high response.

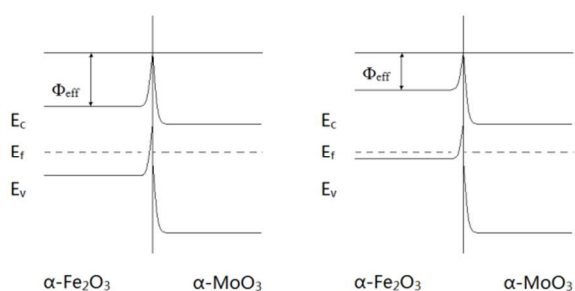


Fig. 10 the energy band structure of the α -MoO₃/ α -Fe₂O₃ heterostructures in air and xylene

Conclusions

In conclusion, α -MoO₃/ α -Fe₂O₃ composites were successfully prepared via a facile two-steps hydro-thermal method. The samples consists of α -MoO₃ nanobelts with length of 6 μ m and width of 200 nm and α -Fe₂O₃ nanorods with length of 10 nm. The mechanism of α -MoO₃/ α -Fe₂O₃ core-shell structural composites to xylene was investigated. Sensors based on α -MoO₃/ α -Fe₂O₃ nanostructure composites were produced and the sensing property was examined. It was found that the sensors based on α -MoO₃/ α -Fe₂O₃ core-shell structural composites showed a higher response related to the sensors based on α -MoO₃ nanobelts to xylene at 206 °C. The result illuminated that α -MoO₃/ α -Fe₂O₃ core-shell nanostructure is a potential candidate for xylene gas sensing.

Acknowledgements

The study was supported by National Natural Science Foundation of China (Grant No. 61274068), National High Technology Research and Development Program of China (Grant No. 2013AA030902), Opened Fund of the State Key Laboratory on Integrated Optoelectronics (No. IOSKL2013KF10) and Postdoctoral Sustainment Fund of Jilin Province (Grant No. RB201371).

Notes and references

^a State Key Laboratory on Integrated Optoelectronics, Jilin University, Changchun 130012, China

^b College of Electronic Science and Engineering, Jilin University, Changchun 130012, China

^c College of Instrument Science and Electrical Engineering, Jilin University, Changchun 130012, China

1. C. E. Davis, C. K. Ho, R. C. Hughes and M. L. Thomas, *Sensors and Actuators B: Chemical*, 2005, **104**, 207-216.
2. J. Hue, M. Dupoy, T. Bordy, R. Rousier, S. Vignoud, B. Schaerer, T. H. Tran-Thi, C. Rivron, L. Mugheri and P. Karpe, *Sensors and Actuators B: Chemical*, 2013, **189**, 194-198.
3. T. Akiyama, Y. Ishikawa and K. Hara, *Sensors and Actuators B: Chemical*, 2013, **181**, 348-352.
4. Y. Chen, L. Zhu, C. Feng, J. Liu, C. Li, S. Wen and S. Ruan, *Journal of Alloys and Compounds*, 2013, **581**, 653-658.
5. H.-M. Jeong, H.-J. Kim, P. Rai, J.-W. Yoon and J.-H. Lee, *Sensors and Actuators B: Chemical*, 2014, **201**, 482-489.
6. Z. Zhang, R. Yang, Y. Gao, Y. Zhao, J. Wang, L. Huang, J. Guo, T. Zhou, P. Lu, Z. Guo and Q. Wang, *Scientific reports*, 2014, **4**, 6797.

7. Y. Wang, X. Zhang, Z. Luo, X. Huang, C. Tan, H. Li, B. Zheng, B. Li, Y. Huang, J. Yang, Y. Zong, Y. Ying and H. Zhang, *Nanoscale*, 2014, **6**, 12340-12344.
8. D. Wang, N. Liu, J. Zhang, X. Zhao, W. Zhang and M. Zhang, *Journal of Molecular Catalysis A: Chemical*, 2014, **393**, 47-55.
9. Y. Meng, T. Wang, S. Chen, Y. Zhao, X. Ma and J. Gong, *Applied Catalysis B: Environmental*, 2014, **160-161**, 161-172.
10. X. Zhang, C. Luo and J. Tang, *Sensors*, 2013, **13**, 15209-15220.
11. N. Datta, N. S. Ramgir, S. Kumar, P. Veerender, M. Kaur, S. Kailasaganapathi, A. K. Debnath, D. K. Aswal and S. K. Gupta, *Sensors and Actuators B: Chemical*, 2014, **202**, 1270-1280.
12. M. B. Rahmani, S. H. Keshmiri, J. Yu, A. Z. Sadek, L. Al-Mashat, A. Moafi, K. Latham, Y. X. Li, W. Wlodarski and K. Kalantar-zadeh, *Sensors and Actuators B: Chemical*, 2010, **145**, 13-19.
13. Z. Hongmei, X. Jianjian, Z. wenjin and H. Wei, *Displays*, 2014, **35**, 171-175.
14. Z. Yin, X. Zhang, Y. Cai, J. Chen, J. I. Wong, Y. Y. Tay, J. Chai, J. Wu, Z. Zeng, B. Zheng, H. Y. Yang and H. Zhang, *Angewandte Chemie*, 2014, **53**, 12560-12565.
15. X. Zhang, X. Zeng, M. Yang and Y. Qi, *ACS applied materials & interfaces*, 2014, **6**, 1125-1130.
16. C. Liu, Z. Li and Z. Zhang, *Electrochimica Acta*, 2014, **134**, 84-91.
17. F. Jiang, W. Li, R. Zou, Q. Liu, K. Xu, L. An and J. Hu, *Nano Energy*, 2014, **7**, 72-79.
18. A. D. Rushi, K. P. Datta, P. S. Ghosh, A. Mulchandani and M. D. Shirsat, *The Journal of Physical Chemistry C*, 2014, **118**, 24034-24041.
19. S. Bai, S. Chen, L. Chen, K. Zhang, R. Luo, D. Li and C. C. Liu, *Sensors and Actuators B: Chemical*, 2012, **174**, 51-58.
20. W.-S. Kim, H.-C. Kim and S.-H. Hong, *Journal of Nanoparticle Research*, 2009, **12**, 1889-1896.
21. Y. H. Cho, Y. N. Ko, Y. C. Kang, I.-D. Kim and J.-H. Lee, *Sensors and Actuators B: Chemical*, 2014, **195**, 189-196.
22. L. Wang, P. Gao, D. Bao, Y. Wang, Y. Chen, C. Chang, G. Li and P. Yang, *Crystal Growth & Design*, 2014, **14**, 569-575.
23. L. Brigo, M. Cittadini, L. Artiglia, G. A. Rizzi, G. Granozzi, M. Guglielmi, A. Martucci and G. Brusatin, *Journal of Materials Chemistry C*, 2013, **1**, 4252.
24. C. Feng, W. Li, C. Li, L. Zhu, H. Zhang, Y. Zhang, S. Ruan, W. Chen and L. Yu, *Sensors and Actuators B: Chemical*, 2012, **166-167**, 83-88.
25. D. Jiang, Y. Wang, W. Wei, F. Li, Y. Li, L. Zhu, C. Feng, C. Liu and S. Ruan, *RSC Adv.*, 2015, **5**, 18655-18659.
26. L. Li, P. Gao, M. Baumgarten, K. Mullen, N. Lu, H. Fuchs and L. Chi, *Advanced materials*, 2013, **25**, 3419-3425.
27. F. Qu, C. Feng, C. Li, W. Li, S. Wen, S. Ruan and H. Zhang, *International Journal of Applied Ceramic Technology*, 2014, **11**, 619-625.